4 Experimental Details

This chapter explains some of the general principles behind the characterization of the devices detailed in the following chapters.

4.1 Standard Characterization Methods

The simple process of attaching a pair of leads to either end of a piece of semiconductor material, passing a current through them, and measuring the voltage developed across them, is generally not sufficient for any accurate characterization. The value of the resistance of the leads and contacts is an unknown variable, but if it is known to be small compared to the resistance of the sample, then meaningful qualitative results can be obtained from this 2-terminal approach.

For quantitative results, it is necessary to use a 4-terminal approach: current is passed along the sample between two contacts, and the voltage across two other contacts is measured. The simplest arrangement for performing this measurement involves having a bar-shaped sample, with the current passing along the long axis: if the aspect ratio is sufficiently large, and the voltage probes are not too near the ends, then the resistivity can be found very easily.[1] It is important to make sure that the contact resistances are not too high, that the impedance of the voltage measurement equipment is as high as possible.

4.1.1 Drift Mobility

Reference has been made in the introductory chapters to the mobility of the charge carriers within the material in terms of the rate at which they undergo scattering events. In terms of the measurement process, however, the mobility is defined by the drift velocity that the carriers reach when subjected to a given electric field, and is therefore sometimes explicitly referred to as the drift mobility:

$$\mu = \frac{|\boldsymbol{v}|}{|\boldsymbol{E}|} \qquad 4.1$$

where $\boldsymbol{v}$ is the drift velocity of the carriers and $\boldsymbol{E}$ is the applied electric field. If the applied current is I, the measured voltage is V, the sheet charge density is qn_S,* the distance between the voltage probes is l and the width of the sample is w, then

$$\mu = \frac{I}{V q n_S} \cdot \frac{l}{w} \qquad 4.2$$

In simple cases, the sheet charge density can be calculated using the Hall effect.

4.1.2 Classical Hall Effect

The most widely used test of electrical quality of semiconductor materials is the Hall measurement.[2] The simplest case concerns a material in which a single carrier is responsible for passing the current through a material with isotropic energy bands and energy-independent scattering mechanisms.

Single Carrier Classical Hall Effect

Using Ohm's law, we define the resistance along the direction of current as

$$R_{XX} = \frac{V_X}{I_X} \qquad 4.3$$

For a 2-dimensional system, this is converted into a "sheet resistivity" by correction for the aspect ratio of the device:

* Since we are concerned with a 2-dimensional carrier gas, it is convenient to refer to a "sheet carrier density" n_S (with dimensions of number per area) rather than a volume carrier density. The use of n_S for the carrier density does not necessarily imply n-type conduction.

$$\rho_{XX} = \frac{V_X}{I_X} \cdot \frac{w}{l} \tag{4.4}$$

Even though w/l is dimensionless, sheet resistivity is generally specified as Ohms per square. The scalar ρ_{XX} ($=\rho_{YY}$) is the diagonal component of the resistivity tensor defined by $\boldsymbol{E} = \rho \boldsymbol{J}$, and the off-diagonal element ρ_{XY} ($=-\rho_{YX}$) becomes non-zero in the presence of a magnetic field $\boldsymbol{B}$ as summed up in the Lorentz force law $\boldsymbol{F} = q(\boldsymbol{E} + \boldsymbol{v} \wedge \boldsymbol{B})$. In the Hall bar under consideration (with $\boldsymbol{B} = (0,0,B)$ and $\boldsymbol{v} = (v,0,0)$) a stable condition is eventually reached ($\boldsymbol{F}=0$) when $E_Y = vB$. Then, the velocity v of the carriers is related to the current I by $I = nqvA = nqvwt = n_S qvw$.

The voltage produced across the Hall bar by the electric field is the Hall Voltage, $V_H = E_y w$, which can be related back to the magnetic field and current:

$$V_H = \frac{I}{n_S qw} \cdot B \tag{4.5}$$

Finally, the off-diagonal component of the resistivity tensor can be found, and the Hall coefficient R_H can be defined.

$$\rho_{XY} = \frac{V_H}{I} = \frac{B}{n_S q} = R_H B \tag{4.6}$$

From this, an expression for finding the sheet carrier density in terms of known or measured quantities can be deduced:

$$n_S = \frac{IB}{qV_H} \tag{4.7}$$

Since the mobility of the carriers (Equation 4.1) relates back to the conductivity by $\sigma = nq\mu$ then in low magnetic field where $\mu B \ll 1$:

$$\rho_{XX} = \frac{1}{n_S \, q \, \mu} \qquad 4.8$$

So, finally:

$$\mu = \frac{1}{n_S \, q \, \rho_{XX}} = \frac{1}{B} \cdot \frac{V_H}{V_X} \cdot \frac{l}{w} \qquad 4.9$$

Based on these simple calculations, the sheet resistivity ρ_{XX} and Hall coefficient R_H are functions of carrier density and mobility and are constant with respect to the magnetic field. However, it is rarely the case that this simple model is directly applicable. In cases where this simple model has been applied without consideration, the properties calculated can be referred to as the *Hall* sheet density and mobility, sometimes denoted as n_H (or p_H for hole-like conduction) and μ_H.

Generalized Classical Hall Effect

The resistance ρ and Hall coefficient R_H vary with magnetic field if there are two or more distinct carrier gases present in the material, or if the carrier gases feature a spread of mobilities. In general,[3]

$$\sigma_{XX}(B) = \int_{-\infty}^{\infty} \frac{s(\mu)}{1 + \mu^2 B^2} \, d\mu \qquad 4.10$$

and

$$\sigma_{XY}(B) = \int_{-\infty}^{\infty} \frac{\mu B s(\mu)}{1 + \mu^2 B^2} \, d\mu \qquad 4.11$$

where

$$s(\mu) = n_S(\mu) \, q \, \mu \qquad 4.12$$

is a generalized conductivity function, and $n_S(\mu)$ represents the mobility spectrum of carriers throughout the material. The experimentally measured parameters are related to the elements of the conductivity tensor by:

$$\rho(B)=\rho_{XX}=\frac{\sigma_{XX}}{\sigma_{XX}^2+\sigma_{XY}^2} \quad 4.13$$

$$R_H(B)=-\frac{\rho_{XY}}{B}=-\frac{1}{B}\frac{\sigma_{XY}}{\sigma_{XX}^2+\sigma_{XY}^2} \quad 4.14$$

The variation of resistance with magnetic field is known as magnetoresistance. In general, classical magnetoresistance is always positive, meaning that the resistance increases with magnetic field.

Assuming a single, ideal carrier gas is equivalent to using an $n_S(\mu)$ of the form of a single delta function, and the result of the previous section is recovered. By using a function for $n_S(\mu)$ whose form comprises a pair of delta functions, the two-carrier Hall coefficient can be found. The Hall coefficient for a two carrier system at low fields, $\mu B \ll 1$, is given by

$$R_H=\frac{\pm n_1\mu_1^2 \pm n_2\mu_2^2}{q(n_1\mu_1+n_2\mu_2)^2} \quad 4.15$$

which becomes

$$R_H=\frac{1}{q(\pm n_1 \pm n_2)} \quad 4.16$$

at high fields, where $\mu B \gg 1$, unless $n_1 \sim -n_2$ (when the condition that $\sigma_{XY} \gg \sigma_{XX}$ breaks down). Positive and negative signs refer to hole and electron transport respectively. Hence, a single carrier model calculation based on the measurement of a two carrier system at low field would yield μ_H and n_H such that

$$\mu_H=\frac{|\pm n_1\mu_1^2 \pm n_2\mu_2^2|}{n_1\mu_1+n_2\mu_2} \quad 4.17$$

and $$n_H = \frac{(n_1 \mu_1 + n_2 \mu_2)^2}{\pm n_1 \mu_1^2 \pm n_2 \mu_2^2}$$ 4.18

Even single carrier systems with an isotropic effective mass can exhibit magnetoresistance, and this is most commonly due to energy-dependent scattering mechanisms. The Hall scattering factor r is given by

$$r = \langle \tau^2 \rangle \Big/ \langle \tau \rangle^2$$ 4.19

where τ is the scattering time, and the angle brackets refer to averaging over energy.

at low fields $$R_H = \frac{r}{n_S q}$$ 4.20

but at high fields $$R_H = \frac{1}{n_S q}$$ 4.21

as before. Equations 4.16 and 4.21 are essentially the same: at high fields, the Hall coefficient depends only on the total charge density in the system. If two carrier gases are present, each with some sort of anisotropy or energy dependent scattering mechanisms, then at low fields both Equations 4.15 and 4.20 apply, and the problem becomes intractable. In fact, the distinction between the existence of multiple carrier gases and the existence of a single carrier gas with a range of properties can become a matter for convention rather than physics in real materials; this distinction may be obvious when considering spatially separate carrier gases but not if, for example, multiple subbands are occupied within the same spatial region of the device at finite temperature.

Computationally intensive methods must be employed to invert Equations 4.10 and 4.11 without making assumptions regarding the form of $n_S(\mu)$ provided at least that μ itself is not a function of magnetic field.[3,4]

In the low temperature degenerate limit there is no broadening of the Fermi-Dirac occupation function in terms of energy, so the Hall scattering factor r~1. As temperature increases, the carriers' energy spreads so the effects of energy-dependent scattering become apparent. In this case, the Hall factor tends to be greater than unity.

Alternatively, the Hall factor can deviate from unity if the energy bands are anisotropic, leading to anisotropy in the effective mass. This consideration is especially relevant in strained layers, such as a silicon-germanium alloy grown epitaxially on a silicon substrate, where the strain breaks the symmetry of the energy bands. In this case, the Hall factor is not necessarily greater than unity.

Figure 4.1 shows magnetoresistance calculated for a number of systems, summarized in Table 4.1. The carrier gases are represented by Gaussians $n_S(\mu)$ of full-width $\Delta\mu_i$ centred at μ_i normalized such that:

$$\int_{-\infty}^{\infty} n_S(\mu)\, q\,\mu\, d\mu = n_i\, q\, \mu_i \qquad 4.22$$

	$\mu_1/cm^2V^{-1}s^{-1}$	$\Delta\mu_1/cm^2V^{-1}s^{-1}$	n_1 / 10^{12} cm^{-2}	$\mu_2/cm^2V^{-1}s^{-1}$	$\Delta\mu_2/cm^2V^{-1}s^{-1}$	n_2 / 10^{12} cm^{-2}
(a)	5000	1000	4.0			
(b)	2000	1000	5.0	5000	1000	2.0
(c)	2000	10	5.0	5000	10	2.0
(d)	-2000	1000	-5.0	5000	1000	2.0

Table 4.1 Parameters used to generate the magnetoresistance curves of Figure 4.1.

Magnetoresistance features appear on a scale of $B \sim 1/\mu$, so the presence of multiple high-mobility gases gives rise to magnetoresistance effects at low fields, whereas a range of mobilities within a single gas causes effects at much larger field scales.

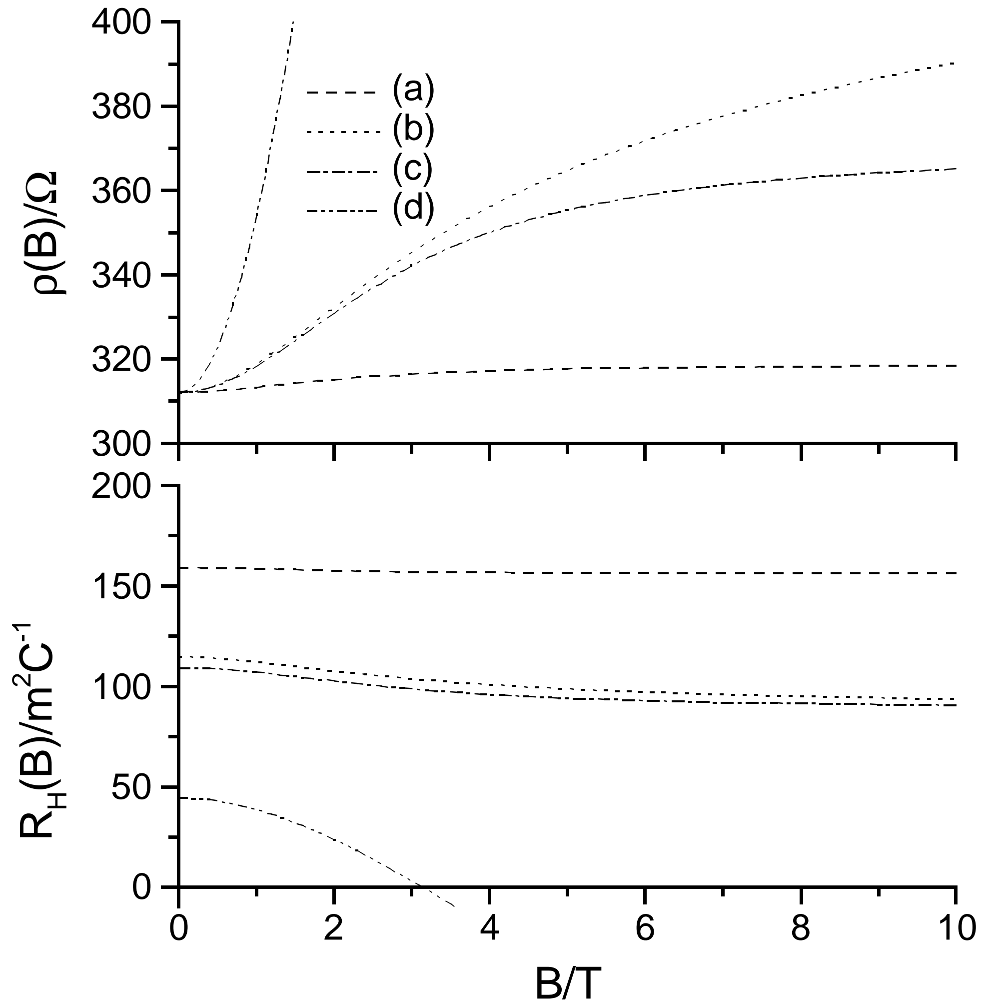

Figure 4.1 Magnetoresistance calculated for four different systems. They are (a) a single carrier gas with a large mobility width, (b) two carrier gases with large width, (c) two "ideal" gases and (d) two gases, one of which contains carriers of the opposite charge (represented by a "negative" mobility and sheet density).

Also, the presence of two carrier gases with opposite charge (that is, electrons and holes) causes very large magnetoresistance and the eventual reversal of the sign of R_H.

4.1.3 Quantum Effects at High Magnetic Fields

In a perfect (that is, non-scattering) semiconductor in the zero temperature limit, the application of a perpendicular magnetic field would cause the carriers to execute cyclotron orbits. The conductivity of the sample would be zero. Current will only flow if the cyclotron motion is interrupted by scattering events.

Expressing this more formally, the presence of a perpendicular magnetic field such that $\hbar\omega_c \geq kT$ where ω_c is the cyclotron frequency qB/m^* leads to the formation of Landau levels. Landau levels are eigenstates of the Schrödinger equation for a 2D carrier gas in a perpendicular magnetic field, essentially the quantum expression of the semi-classical concept of cyclotron orbits. Ideally the sub-band structure created by Landau levels takes the form of a series of delta functions at energies $E_n = \hbar\omega_c(n+½)$, but in a real system in the presence of scattering the energy can only be defined to within ~ $\hbar/\tau_q$, where τ_q is the quantum lifetime, leading to broadened Landau levels which are only distinct if $\hbar\omega_c \geq kT$. Essentially, this means that for these effects to be relevant, each carrier must have enough time to execute at least one cyclotron orbit between scattering events,[5] ie. $\tau_q > 2\pi/\omega_c$.

As the magnetic field increases, the separation between Landau levels grows, and so does the number of states each contains,[5] eB/h. The position of the Fermi level will move away from its zero-field value, so that the density of the carrier gas remains constant as the number of available Landau levels decreases. The filling factor ν is a measure of the number of filled Landau levels. At integer values of ν the Fermi level is

half way between two Landau levels and there can be no scattering. For a constant carrier sheet density, $\nu \propto 1/B$. In an imperfect system, impurities and crystal defects lead to random potential fluctuations which cause states at the edges of each Landau level to be localized so that they do not contribute to the conductivity of the device.

However, if a carrier begins an orbit very close to the edge of a spatially finite device, then it will hit the edge of the device (a potential barrier) and be scattered; this will lead to a net drift velocity which will be higher the closer the carrier is to the edge. The presence of an edge effectively bends the subband structure upwards in energy. These "edge states" behave as one-dimensional quantum wires and mean that there is conduction even when the Fermi level is positioned between Landau levels in the bulk of the device.

These considerations lead to a completely revised picture of magnetotransport, compared to behaviour in the classical regime.

Figure 4.2 shows data from the sample studied in Chapter 6, a 2-dimensional electron gas confined within a quantum well of pure silicon, sandwiched between relaxed $Si_{0.75}Ge_{0.25}$ layers. The temperature is 350mK; the carriers have a mobility of around 25,000cm^{2}V^{-1}s^{-1} and a sheet density of 8.1×10^{11}cm^{-2}. For fields around 1 or 2 Tesla, Shubnikov-de Haas oscillations (which are periodic in inverse magnetic field) appear. Minima in resistivity appear at filling factors of *4n*, where *n* is an integer. For larger fields, the oscillations first become "spin-split" and then "valley-split," eventually showing minima for all integer *n*.

The spin degeneracy is lifted (spin-splitting is observed) when the Zeeman energy between spin states is greater than the broadening of the Landau Levels. In Figure 4.2 spin-split resistance minima can be seen at ν=10 and ν=6. Thus at higher magnetic fields minima appear at *2n*.

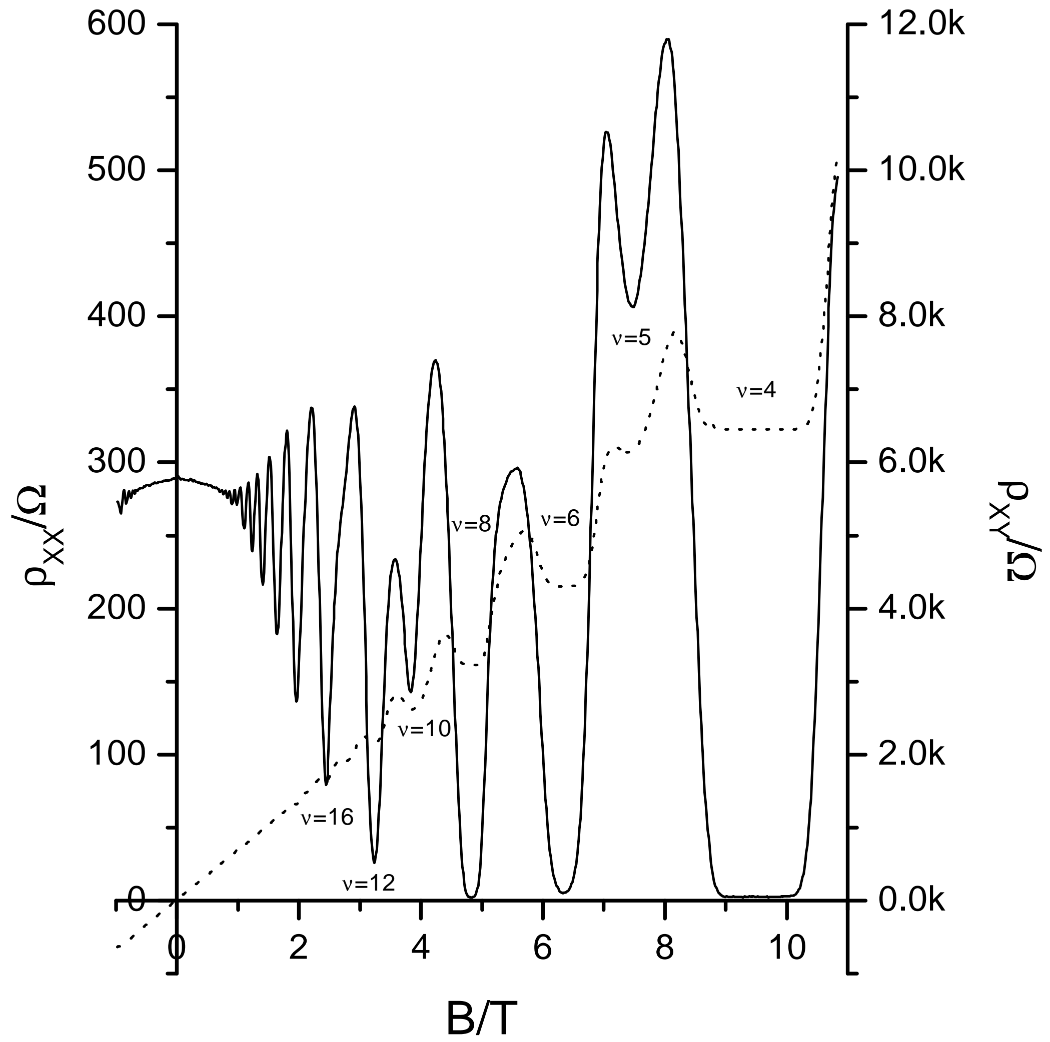

Figure 4.2 A 2DEG showing Shubnikov-de Haas and Quantum Hall Effects at a temperature of 350mK. The dotted line is the transverse resistivity and is associated with the y-axis on the right. Minima in resistivity are labelled with their corresponding filling factors. Conduction is dissipationless at ν=4.

Since the electron has spin ½, in an applied magnetic field they can take a low energy orientation along the field or a high energy orientation against it. The energy difference between these two states is $E_{Zeeman} = g \mu_B B$, with $g = 2.0023$ for a free electron.[6] In the 2DEG the charge carriers are not free electrons, but rather the electron-like quasiparticles that result from the interactions of the electron with other electrons and the silicon lattice. The Landé *g*-factor of electrons in bulk silicon is 1.99[7] but in a 2DEG it is larger and is in general anisotropic[8,9,10,11] and a function of magnetic field and sheet density.[12,13,14] (Values of between 2.6 and 4.2 are reported in Reference 13, found by tilting the magnetic field but ignoring possible anisotropy.) The Zeeman splitting energy can be compared to the Landau level separation $\hbar \omega_c$ and it is found that

$$E_{Landau} = \frac{2}{g} \frac{m_e}{m^*} E_{Zeeman} \qquad 4.23$$

The appearance of a minimum in ρ_{XX} for an odd filling factor (ν=5 at 7.4T) shows that the two-fold valley degeneracy has also been lifted: there is additional degeneracy factor of 2, because in silicon the electrons in the 2DEG occupy two [001]-valleys. The precise origin of valley splitting is not entirely understood, but may be related to the strength of the electric field at the interface which defines the 2DEG. [13]

As the magnetic field reaches 9T, ρ_{XX} drops to zero, but since ρ_{XY} remains finite (and large) then σ_{XX} is also (counterintuitively, but clearly from Equation 4.13) zero and conduction is dissipationless, in accordance with the theory given above which asserts that the conductivity drops to zero when the Fermi level is halfway between two Landau levels. The ρ_{XY} data show classical $\rho_{XY} \propto B$ behaviour for low fields, and integer quantum Hall effect plateaux where the transverse resistance is pinned at $\rho_{XY} = \frac{h}{\nu e^2}$ over a finite magnetic field range, for higher fields.

For holes, where both m^* and g are larger than for electrons,[8] the up-spin state

of one Landau level can be closer in energy to the down-spin state of the next. Since there is no valley degeneracy (there is a single minimum in the band at $|\boldsymbol{k}|=0$) then minima which are not spin-split would appear at odd filling factors.

Shubnikov-de Haas oscillations are very useful, because their period in inverse magnetic field can be used to determine the true carrier sheet density, in contrast to Hall measurements which may be invalidated by the anisotropy of the band structure, for example. Their decay with increasing temperature can be used to determine the effective mass of the carriers, and their amplitude with respect to magnetic field can be used to determine the ratio α between the quantum lifetime τ_q (the time taken for a particle to scatter elastically to any other state) and the transport lifetime τ (which recognises that small angle scattering has little bearing on the drift velocity, whilst large angle scattering does; referred to explicitly as τ_{tr} when necessary for clarity).

If the Landau levels are assumed to be broadened into Lorentzians each with a width $\hbar/2\tau_q$ then the resistivity of a 2-dimensional carrier gas subject to a perpendicular magnetic field at low temperatures is given by:[15]

$$\rho_{XX}(B,T)=\rho_0(T)\left[1+4\sum_{s=1}^{\infty}\frac{s\,\xi(B,T)}{\sinh[s\,\xi(B,T)]}\cdot e^{\frac{-\pi\alpha s}{B\mu(T)}}\cdot\cos\left(2s\pi^2\frac{\hbar n_S}{qB}-s\pi\right)\right] \quad 4.24$$

with

$$\xi(B,T)=\frac{2\pi^2 kTm^*}{eB\hbar} \quad 4.25$$

and

$$\alpha=\frac{\tau_{tr}}{\tau_q} \quad 4.26$$

provided that the oscillations are small. The $s>1$ terms in the summation are only relevant for very high mobility samples, so only $s=1$ will be considered. The cosine term represents the oscillations themselves, and if their period in inverse magnetic field

is $\Delta(1/B)$ then the sheet density n_S can be extracted using

$$n_S = \frac{q}{\pi\hbar\Delta(1/B)} \qquad 4.27$$

The exponential term controls the amplitude of the oscillations with respect to magnetic field (in the zero temperature limit) depending on how many cyclotron orbits each carrier executes between scattering events.

The term $s\xi(B,T)/\sinh[s\xi(B,T)]$ thermally damps the oscillations.

In order to find m^* and α, first it is necessary to pick out the maxima and minima of the oscillations (using magnetic fields values between the onset of oscillations up to spin-splitting) for a number of temperatures, and subtract the slowly varying classical magnetoresistance background. This leaves a set of amplitudes of the oscillations themselves, $\delta\rho_{mm}(B,T)$.

Assume a value (for example, unity) for α and then consider $\delta\rho_{mm}(T)$ at a particular B: A plot of

$$\ln(\delta\rho_{mm}) \quad \text{vs.} \quad \ln\left(\frac{\rho_0(T)\xi(m^*,T)}{\sinh\xi(m^*,T)}\right) - \left(\frac{\pi\alpha}{\mu(T)B}\right) \qquad 4.28$$

will have a gradient of unity and an intercept of ln(4) if the choice of m^* is correct. $\rho_0(T)$ is the Boltzmann resistivity: the value of $\rho_{XX}(B=0,T)$ may be used, or the value of $\rho_{XX}(T)$ at the field just before oscillations become visible. If no temperature dependence is assumed, then

$$\ln(\delta\rho_{mm}) \quad \text{vs.} \quad \ln\left(\frac{\xi(m^*,T)}{\sinh\xi(m^*,T)}\right) \qquad 4.29$$

is plotted instead. Data from maxima and minima at many magnetic fields should be averaged.

This effective mass can then be used in a plot of

$$\ln\left[\left(\frac{\sinh\xi}{\xi}\right)\cdot\left(\frac{\delta\rho_{mm}}{\rho_0}\right)\right] \quad \text{vs.} \quad \frac{1}{\mu B} \qquad 4.30$$

for $\delta\rho_{mm}(B)$ at a particular temperature. These points should lie on a line with a gradient of $-\pi\alpha$ and an intercept again of ln(4). This α should be used to determine a better value for m^*, and iterations should continue until satisfactory fits for both parameters are found.[16]

Since τ_q considers all elastic scattering events to be equally important but τ_{tr} considers that the most important events are those that lead to the greatest change in the direction of the wavevector, it is generally the case that $\tau_q < \tau_{tr}$ and thus that $\alpha > 1$. For example, scattering from remote impurities is predominantly small-angle so leads to a value of α greater than unity (in $GaAs/Ga_{1-x}Al_xAs$ heterostructures the value of α can be of the order 10) whilst scattering from a rough interface tends to lead to $\alpha \sim 1$.[17]

4.1.4 Quantum Effects at Low Magnetic Fields

In a disordered semiconductor where $k_B T \ll E_F$, the transport properties of a 2-dimensional carrier gas may reflect the quantum nature of the charge carriers even in the absence of a field strong enough to form Landau levels. (These effects can usually be generalized to other dimensionalities).

Weak localization

Figure 4.3 shows a particle which is scattered around in a loop, due to disorder

in the system: each scattering event corresponds mainly to a change in the direction of the momentum with only a small change in energy. By definition, these happen on a timescale of the elastic scattering time (or quasi-particle lifetime) τ. In quantum mechanical terms, this means the wavefunction of the particle interferes with itself at the intersection point. The wavefunction must be single valued at this point, so the probability current cannot cross itself. Instead, three paths are possible; part of the current will ignore the loop entirely and continue unscattered, part of the current will travel around the outside of the loop, and the remaining part will remain trapped within the loop.

If a scattering event occurs which changes the energy of the particle significantly (and therefore breaks the time-reversal symmetry of the loop) then the phase coherence of the wavefunction will be broken, the quantum mechanical constraint will be relaxed, and the particle will no longer be localized. Events like this occur on a timescale of the dephasing time τ_φ which is related to the inelastic scattering time.[18] The maximum loop size is therefore set by τ_φ whilst the minimum loop size is set by τ.

A magnetic field applied perpendicular to the plane of the carrier gas will serve to change the phase of the wavefunction around the loop. Larger loops will be the most affected since they will enclose more flux.

The correction to the Boltzmann conductivity in the diffusive limit $\tau \ll \tau_\psi$ is given by[19]

$$\delta\sigma_{xx}^{loc}(B) = -\frac{e^2}{2\pi^2\hbar}\left[\Psi\left(\frac{1}{2}+\frac{\hbar}{4eBD\tau}\right)-\Psi\left(\frac{1}{2}+\frac{\hbar}{4eBD\tau_\psi}\right)\right] \qquad 4.31$$

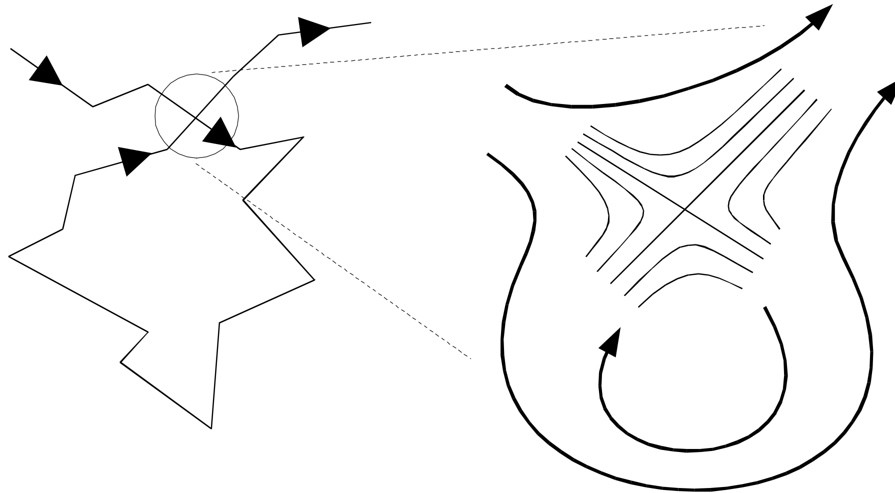

Figure 4.3 A schematic representation of weak localization. On the left, a classical trajectory featuring a loop is shown. However, in quantum-mechanical terms the wave-function must be single valued at the intersection point (shown on the right: fine lines represent equal-probability contours) and part of the probability current (shown by arrows) becomes localized in the loop. Inelastic scattering will destroy the time-reversal symmetry and break this coherence, whilst a magnetic field through the loop will change the phase of each of the paths relative to each other.

with the diffusion constant $D=\frac{E_F \mu}{e}$ and the digamma function (related to the Gamma function *Γ(x)*) $\Psi(x)=(\ln[\Gamma(x)])'=\frac{\Gamma'(x)}{\Gamma(x)}$. In the limit of low field, this reduces to[20]

$$\delta\sigma_{xx}^{loc}(0)=-\frac{e^2}{2\pi^2\hbar}\ln\left(\frac{\tau_\psi}{\tau}\right) \qquad 4.32$$

The transverse component of the conductivity tensor is then found to be

$$\delta\sigma_{xy}^{loc}(B)=-2\mu B\,\delta\sigma_{xx}^{loc}(B) \qquad 4.33$$

and this result is assumed to hold for all *B*.[21]

Weak localization is quenched when $\mu B\sim\hbar/E_F\tau$: the magnetic flux through the loop described by the weakly-localized carrier is such that the phase change around the loop reaches the order of π even for the smallest allowed loops.

Interactions and Spin-Splitting

Corrections also arise from particle-hole interactions (which are not directly dependent on magnetic field) and the manner in which these interactions are effected by the Zeeman splitting of spin states. The former is given by[18,20,22,23]

$$\delta\sigma_{xx}^{\text{int}}=\frac{e^2}{2\pi^2\hbar}\left(1-\frac{3}{4}F^*\right)\ln\left(\frac{kT}{\hbar/\tau}\right) \qquad 4.34$$

Here, F^* is a renormalized screening parameter

$$F^*=\frac{8}{F}\left(1+\frac{1}{2}F\right)\ln\left(1+\frac{1}{2}F\right)-4 \qquad 4.35$$

where F itself comes from considerations of the exchange and Hartree contributions to the self-energy correction (representing the interaction of a given eigenfunction with the nonuniform electron density in the ground state) and is given by[18,20]

$$F=\int_0^{2\pi}\frac{d\Theta}{2\pi}\left[1+2k_F\frac{2\pi\epsilon_0\epsilon_r\hbar^2}{m^*e^2}\sin(\Theta/2)\right]^{-1} \qquad 4.36$$

The $-\frac{3}{4}F^*$ Hartree term in Equation 4.34 was initially calculated to be simply $-F$, under the assumption that $F\ll 1$ and the addition of this first-order term was therefore valid.[20] The realization, however, that triplet and singlet states should feature in the considerations of particle-hole scattering lead to the replacement of F with $\frac{3}{4}F^*$ in each of the formulae in which it appears. F^* is actually a different function of F depending on which kind of correction one is calculating and the dimensionality: Equation 4.36 is appropriate for 2-dimensional conductivity.[23] Since F can in theory only take values between 0 and 1 (decreasing with increasing sheet density) then F^* can only take values between 0 and 0.866.

The correction to the conductivity due to the Zeeman splitting of spin states (provided that this is greater than their broadening due to very high spin-orbit scattering or spin-flipping rates) is given by[18]

$$\delta\sigma_{xx}^{spin}(B)=-\frac{e^2}{2\pi^2\hbar}\left(\frac{F^*}{2}\right)G\left(\frac{g\mu_B B}{k_B T}\right) \qquad 4.37$$

Here, μ_B is the Bohr magneton, g is the Landé g-factor of the carriers and may in general be anisotropic or field or density dependent. The function G has been evaluated numerically.[24]

Inversion and implicit differentiation of the conductivity tensor leads to the following expression for the magnetoresistance $\Delta\rho_{XX}(B)=\delta\rho_{xx}(B)-\delta\rho_{xx}(0)$ which incorporates the corrections described above:[21]

$$\Delta\rho_{XX}(B)=\rho_0^2\left[(\mu^2B^2-1)\delta\sigma_{xx}^{loc}(B)+\delta\sigma_{xx}^{loc}(0)-4\mu^2B^2\delta\sigma_{xx}^{loc}(B)\right] + \rho_0^2\left[(\mu^2B^2-1)\delta\sigma_{xx}^{spin}(B)+\mu^2B^2\delta\sigma_{xx}^{\mathrm{int}}\right] \qquad 4.38$$

Interaction effects should also lead to corrections in the Hall signal, whereas weak localization effects should not. Also, if the magnetic field is applied parallel to the plane of the 2-dimensional carrier gas then all magnetoresistance terms incorporating μB apart from the Zeeman term should vanish.[21] However, calculations and measurements of the anisotropy of the Landé g-factor suggest that it too vanishes in a parallel magnetic field.[8,9] Applications of this theory will be presented in Chapter 5.

4.2 Measuring Equipment

4.2.1 Room Temperature IV Measurements

Making Contact to Unmounted Samples

It is possible to characterize a semiconductor device at room temperature without disecting a wafer or mounting the chip into a package, by using a needle probing station. The chip is positioned on a stage under a stereoscope. The stage can be moved in both the x and y directions so that the intended device can be brought into view.

Needle probes, which feature a needle that can be moved in the x, y and z directions mounted on a heavy magnetic base, can then be gently (and very carefully) lowered onto the contact pads of the chip. Each probe needle can then be connected to the measurement electronics and the device can be characterized.

IV Measurement with the Hewlett-Packard HP4145 Parameter Analyzer

A HP4145 Parameter Analyzer, specially designed for the characterization of electrically sensitive semiconductor devices, was employed extensively throughout. Applied currents and voltages were limited (generally to the order of microamps and

millivolts drain-source, although higher voltages and smaller currents were necessary for gate terminals) so as not to subject the device under test to harmful extremes, whilst the high input impedance (at least $10^{12}\Omega$) ensured that voltages were measured accurately. Gate voltages were only applied once the source and drain voltages were set: this was particularly relevant to the sensitive Siemens devices described in Chapter 5.

4.2.2 Low Temperature Measurement Issues

Sample Mounting

Initially, small, thin packages with a very small lead spacing were used for the low-temperature characterization of these samples. However, this led to problems with the connection of wires to the sample. Securing the package to the cryostat cold-finger was also unsatisfactory, and since space was not an issue within the closed-cycle cryostat larger 14-pin DIL (Dual InLine) packages were employed instead. These were based on the industry-standard 0.1” pitch, so cheap sockets were available from electronics suppliers. The device could be mounted into its socket once wires were already soldered and all the test equipment connected, so that the device was less at risk from stray and potentially damaging electrical signals. A cryostat block incorporating a 14-pin DIL socket was fabricated, which also solved physical mounting issues.

The process of electrically connecting the sample's contacts to the leads of the package, using an ultrasonic gold-wire ball-bonder, was not entirely reliable. As will be apparent in Chapter 7, not every contact worked at low temperatures. The bonding process may have been responsible for altering the IV characteristics of the contacts. However, provided that the resistances of the contacts remained reasonable any non-linearities should have been corrected for by the 4-terminal method.

Lock-In Amplifiers and Automated Computer Recording.

Lock-in amplifiers were employed mainly for low-temperature, low signal measurements. Computer programs existed for automating the measurement process and recording the lock-in values via the IEEE-488 General-Purpose Inferface Bus (GPIB). Also, a configuration was developed where the HP4148 Parameter Analyser reliably modulated the gate voltage and recorded the analogue output voltages of the lock-in amplifiers, which were measuring the other voltages and currents in the system. This system was both more efficient and safer (for the device) than applying gate voltages manually with a standard Keithley voltage source. Also, when many devices are connected in an IEEE system, one temperamental device can halt the whole measurement and human intervention is required.

Current Heating

Care was taken at every stage to ensure that the current drive through the devices was not causing any significant heating, either of the carriers in relation to the lattice (bringing them out of thermal equilibrium with each other) or of the whole lattice. In general this was performed by checking for Ohmic behaviour in the IV characteristics, but considerations of, for example, the energy loss rates per carrier will be presented where especially relevant.

Cryostats

Two cryostats were employed for the experimental work presented in Chapters 5, 6 and 7. Initially, Hall-effect and low-temperature IV measurements were performed in a closed-cycle cryostat with a base temperature of 10K and a permanent magnet with a field of 0.41T. The permanent magnet was replaced by an electromagnet with a maximum field of 1.2T during the course of these investigations.

More detailed Hall-effect, magnetoresistance and temperature-dependance measurements were made using an Oxford Instruments ^{3}He cryomagnetic system, which allowed more-or-less stable temperatures to be reached between 350mK and ~300K and fields of up to 11T.

1 J. Volger, *Note on the Hall Potential Across an Inhomogeneous Conductor*, Physical Review **79** 1023-1024 (1950)

2 R. A. Stradling and P. C. Klipstein, *Hall, Magnetoresistance and Infrared Conductivity Measurements,* Growth and Characterisation of Semiconductors 165-185, IOP Publishing (1990, 1991).

3 W. A. Beck and J. R. Anderson, *Determination of electrical properties using a novel magnetic field-dependent Hall technique*, Journal of Applied Physics **62** (2) 541-554 (1987)

4 S. Kiatgamolchai, *Maximum-Entropy Mobility Spectrum of Two-Dimensional Hole Gas in Strained-$Si_{1-x}Ge_x$/Si Heterostructures*, Thesis, University of Warwick (2000)

5 J. H. Davies, *The Physics of Low-Dimensional Semiconductors*, Cambridge University Press (1998)

6 P. J. Mohr and B. N. Taylor, *CODATA recommended values of the fundamental physical constants: 1998*, Reviews of Modern Physics **72** (2) 351-495 (2000)

7 D. K. Wilson and G. Feher, *Electron Spin Resonance Experiments on Donors in Silicon. III. Investigation of Excited States by the Application of Uniaxial Stress and Their Importance in Relaxation Processes*, Physical Review **124** (4) 1068-1083 (1961)

8 E. Glaser, J. M. Trombetta, T. A. Kennedy, S. M. Prokes, O. J. Glembocki, K. L. Wang and C. H. Chern, *Detection of Magnetic Resonance on Photoluminescence from a Si/$Si_{1-x}Ge_x$ Strained-Layer Superlattice*, Physical Review Letters **65** (10) 1247-1250 (1990)

9 G. Hendorfer and J. Schneider, g-*factor and effective mass anisotropies in pseudomorphic strained layers*, Semiconductor Science and Technology **6** 595-601 (1991)

10 P. Le Jeune, D. Robart, X. Marie, T. Amand, M. Brousseau, J. Barrau, V. Kalevich and D. Rodichev, *Anisotropy of the electron Landé* g *factor in quantum wells*, Semiconductor Science and Technology **12** 380-383 (1997)

11 A. Malinowski and R. T. Harley, *Anisotropy of the electron* g *factor in lattice-matched and strained-layer III-V quantum wells*, Physical Review B, **62** (3) 2051-2056 (2000)

12 F. F. Fang and P. J. Stiles, *Effects of a Tilted Magnetic Field on a Two-Dimensional Electron Gas*, Physical Review **174** (3) 823-828 (1968)

13 S. J. Koester, K. Ismail and J. O. Chu, *Determination of spin- and valley-split energy levels in strained Si quantum wells*, Semiconductor Science and Technology **12** 384-388 (1997)

14 Th. Englert, D. C. Tsui, A. C. Gossard and Ch. Uihlein, g-*Factor Enhancement in the 2D Electron Gas in GaAs/AlGaAs Heterojunctions*, Surface Science **113** 295-300 (1982)

15 P. T. Coleridge, R. Stoner and R. Fletcher, *Low-field transport coefficients in GaAs/$Ga_{1-x}Al_xAs$ heterostructures*, Physical Review B 3**9** (2) 1120-1124 (1989)

16 A. D. Plews, *Electronic Properties of Two-Dimensional Hole Gases in Si/SiGe Heterostructures*, Thesis, University of Warwick (1996)

17 J. P. Harrang, R. J. Higgins, R. K. Goodall, P. R. Jay, M. Laviron and P. Delescluse, *Quantum and classical mobility determination of the dominant scattering mechanism in the two-dimensional electron gas of an AlGaAs/GaAs heterojunction*, Physical Review B **32** (12) 8126-8135 (1985)

18 P. A. Lee and T. V. Ramakrishnan, *Disordered electronic systems*, Reviews of Modern Physics **57** (2) 287-337 (1985)

19 S. Hikami, A. I. Larkin and Y Nagaoka, *Spin-Orbit Interaction and Magnetotransport in the Two Dimensional Random System*, Progress of Theoretical Physics **63** (2) 707-714 (1980)

20 B. L. Altshuler, D. Khmel' nitzkii, A. I. Larkin and P. A. Lee, *Magnetoresistance and Hall effect in a disordered two-dimensional electron gas,* Physical Review B 3**9** (2) 5142-5153 (1980)

21 M. J. Kearney, *Semiclassical versus quantum magnetotransport in two-dimensional disordered systems*, Semiconductor Science and Technology **7** 804-809 (1992)

22 B. L. Altshuler, A. G. Aronov and P. A. Lee, *Interaction Effects in Disordered Fermi Systems in Two Dimensions*, Physical Review Letters **44** (19) 1288-1291 (1980)

23 P. W. Anderson, E. Abrahams and T. V. Ramakrishnan, *Possible Explanation of Nonlinear Conductivity in Thin-Film Metal Wires*, Physical Review Letters **43** (10) 718-720 (1979)

24 M. S. Burdis and C. C. Dean, *Anomalous values of interaction constants in the two-dimensional electron gas of a silicon metal-oxide-semiconductor field-effect transistor measured by parallel- and perpendicular-field magnetoconductivity*, Physical Review B **38** (5) 3269-3275 (1988)